International Journal of Luminescence and applications
Vol6 (3) September, 2016, pages 172-182

PHOTOLUMINESCENCE STUDY OF $TiO_2:Eu^{3+}$ @ SiO_2 CORE-SHELL AND PURE PHASES OF TiO_2 NANOPARTICLES

Th.Nando Singh[1], Th.Gomti Devi [1] and Sh.Dorendrajit Singh[2]
[1]Department of Physics, NERIST, Nirjuli-791 109, Arunachal Pradesh
[2]Department of Physics, Manipur University, Canchipur-795 003, Manipur
Email: thoudam.nando@gmail.com, dorendrajit@yahoo.co.in

Abstract

$TiO_2:Eu^{3+}$ @ SiO_2 core-shell and pure phases of titanium dioxide(TiO_2)nanoparticles have been successfully synthesized by non-aqueous sol-gel method by using titanium isopropoxide(TIP) and ethanol as the main precursor materials. Transition Electron Microscopy(TEM) image shows well separated distinct particles. The crystal structures were studied using x-ray diffraction(XRD) and found to observe sizes in the range 5-15nm which is almost similar to the TEM analysis results. The luminescence study of europium doped titania nanoparticles show a strong red emission at 617nm originating from the $^5D_0 \rightarrow {}^7F_2$ transition of Eu^{3+} ions. After reaching optimum emission intensity at a specific concentration,decrease in luminescence intensity was observed due to concentration quenching effect.

Keywords:*Core-shell,,TEM, Photoluminescence,Charge transfer, Lifetime*

1.0 INTRODUCTION

Titanium dioxide (TiO_2) is highly ionic white metaloxide n–type semiconductor material with diverse range of applications ranging from medicine, chemical to electronic industries [1-4]. It has been widely used in photocatalysis [5], photovoltaic cells [6], humidity sensors [7], Li ion batteries [8], solar cells [9], hydrogen storage [10], bio-medical engineering [11], drug delivery systems, antibacterial materials, cosmetics, sunscreens, and electronics [12], nontoxic [13], etc. It has four polymorphs in nature, including rutile (tetragonal), anatase (tetragonal) [1-2], brookite (rhombohedral) [3], and TiO_2 (B) (monoclinic). Other high pressure polymorphs have been also reported [14]. Rutile is more stable than anatase and brookite. Anatase and rutile adopted tetragonal symmetry with space group $I4_1/amd$ and $p4_2/mnm$ respectively, p_{bca} and c_2/m for brookite and TiO_2 (B) respectively. TiO_2 is a wide band gap semiconductor with a band gap energy of 3.2 eV for the anatase crystal structure, and 3.0 eV for the rutile structure [15]. This wide band gap of TiO_2 is adequate for doping with lanthanides so that the 4f state lies within the gap which decreases the probability of non-radiative de-excitation mechanism [16]. Rutile is in the stable phase at high temperature, and is obtained in most attempts to grow TiO_2 crystals.

Rutile is the most extensively investigated form of titanium dioxide. Nevertheless, the anatase phase can also be stabilized in the form of powders, ceramics, natural or synthetic crystals, thin films, etc. The availability of two slightly different crystal structures for a same oxide provides a good opportunity to test our understanding of the electronic properties related to their structure. The increasing interest in anatase is demonstrated by the recent successful application of colloidal anatase in a novel photochemical solar cell [9].

The development of systematic studies for the synthesis of oxide nanoparticles is current challenge, the preparation method may be grouped in two streams based upon liquid-solid [17] and gas-solid [18] nature of the transformation. In this paper, we have used the nonaqueous sol-gel method to prepare the TiO_2 compound which is under liquid-solid transformation [19-23]. We have prepared undoped and Eu^{3+} doped TiO_2 nanoparticles upto 1 at. % of Eu^{3+} and characterized them for their structural and luminescence properties. This method is very important for the synthesis of titania nanoparticle. It provides compositional homogeneity that can control the structural morphology and grain size of the particles. The result of low temperature sol-gel synthesis is amorphous in most cases and hence we require various processes to bring to crystallization state. To overcome these specific problems in hydrolytic system, sol-gel process of non-hydrolytic system have been developed. Various research groups have worked on low temperature process [24-25]. However, further study using different route and precursors is necessary to investigate new nanoparticles which have efficient properties in photocatalytic activities. Hence our work based on low temperature non-aqueous route is chosen for the study. The sol-gel synthesis process involves hydrolysis and condensation reaction as two important steps. In aqueous sol-gel process, the oxygen for the formation of the oxidic compound is supplied by the water molecules. In non-aqueous

process, where intrinsically, no water is present, the question of the oxygen for the metal oxide arises. So the oxygen for nanoparticle formation is provided by the solvent EtOH or titanium alkoxide[25].

2.0 Materials

The starting materials used in this study weretitanium(IV) isopropoxide (TIP) [$Ti(OCH(CH3)_2)_4$, with purity 98+%, Acros Organics, Newjersey, U.S.A, europium (III) oxide[Eu_2O_3, with purity 99.99%, HIMEDIA], absolute ethanol (EtOH) [C_2H_5OH, with purity 99.8%, HIMEDIA], sodium hydroxide [NaOH] and concentratic hydrochloric acid [HCl with purity 35%, HIMEDIA]. All the chemicals were used in a reagent grade and used without further purification.

2.1 Method

The sol–gel processing method was used for the synthesis of undoped TiO_2 and europium ion doped TiO_2 (TiO_2:Eu^{3+}) nanoparticles. To prepare undoped TiO_2, 0.5ml of 0.1M HCl was dissolved in 25ml of EtOH. This mixture was labelled as A. 25ml ofEtOH was added dropwise in 5ml of TIP under constant stirring using magnetic stirrer in an ice bath at 5°C. The pH of this mixture was adjusted to~8 by using NaOH and HNO_3 and labelled as B. Mixture A was added dropwise into mixture B under constant stirring at 5°C. This mixture solution was clear and transparent then white precipitate was appeared. After 10 minutes, it turned into gel. The gel was left for ageing for two hours. The gel was collected for centrifugation after adding sufficient amount of EtOH and washing many times. The resultant gel was dried in a hot air oven at 90°C for 16 hours. Finally the dried product was annealed at 220, 350, 450, 550°C for two hours. For a typical synthesis of 0.4 at. % Eu^{3+} ion doped TiO_2, 0.5ml of 0.1M HCl and 25ml of EtOH were mixed. This mixture was introduced dropwise into the vigorously stirred mixture of 5ml of TIP and 25ml of EtOHuntil milky white precipitate was obtained and pH value was adjusted at ~ 8 using NaOH and HNO_3 again 0.0231g of Eu_2O_3 prepared solution is added. Two necked round bottom flask of 500ml was used to remove excess HCl by evaporation and diluted with distilled water for the preparation of Eu_2O_3 prepared solution. The resulting precipitate quickly becomes gel. The gel was left for ageing for two hours. Then the gel was collected for centrifugation after adding sufficient amount of EtOH and washed many times with EtOH. Then the gel was dried in a hot air oven at 90°C for 16 hours. Finally the dried product was annealed at 350, 450, 550°C for two hours. Similar processes were adopted for the preparation of other samples.

2.2 Characterization

Powder X-ray diffraction (XRD) studies were performed using Ultima IV X-Ray diffractometer, Rigaku with nickel filtered CuKα radiation (λ=1.5406Å). The crystallite size (d) was evaluated using Debye - Scherer relation [26]:

$$d = K\lambda/(\beta cos\theta) \qquad (2.1)$$

where β is the full width at half maximum (FWHM) of the diffraction peak in radian; λ (=0.15406nm) is the wavelength of x-ray for CuKα; θ is the Bragg's angle measured in radian; k is a constant taken as 0.89 and known as structural constant. Average crystallite size was computed with the used of Williamson and Hall equation [27]:

$$\beta cos\theta = \lambda/\varepsilon + \eta sin\theta \qquad (2.2)$$

where ε is the average crystallite size; η is the strain; λ is the incident x-ray wavelength (0.15406 nm); β(measured in radian) is the FWHM of the XRD peak and θ is the Bragg's angle in radian. The phase content of a sample can be determined from the weight fraction of rutile (W_R) generally known as Spur and Mayer [28] relation if the sample contains only anatase and rutile:

$$W_R = I_R/(0.884I_A + I_R) \qquad (2.3)$$

where I_A represents the integrated intensity of the anatase(101) peak, and I_R the integrated intensity of rutile(110) peak. The weight fraction of anatase(W_A) and rutile(W_R) in antase – rutile mixture are found to observe 0.5 and 0.56 respectively.

Transmission electron microscope (TEM) images were carried out using JEOL JEM 2100(200kV), Fourier transform infra-red (FT-IR) spectra were recorded in IRAffinity-1 (Shimadju), Raman Spectra were recorded using 785nm Xplora1 micro Raman system, UV-visible spectra were recorded in UV-2600, UV-vis Spectrophotometer (Shimadzu) and optical band gap energy (E_g) of the nanoparticles were calculated from Tauc relation:

$$\alpha h\vartheta = A(h\vartheta - E_g)^m \qquad (2.4)$$

where α is the linear absorption coefficient of the material given by Beer - Lambert's law, A is an energy-independent constant, ϑ is frequency and m is a constant which determines the type of optical transitions: for indirect allowed transition, m = 2; for indirect forbidden transition, m= 3; for direct allowed transition, m = 1/2; and for direct forbidden transition, m = 3/2. Excitation and PL emission spectra of prepared Eu^{3+} ion doped TiO_2 nanoparticles were measured on Perkin Elmer LS 55 Fluorescence Spectrometer.

3. RESULTS AND DISCUSSION

3.0 XRD study

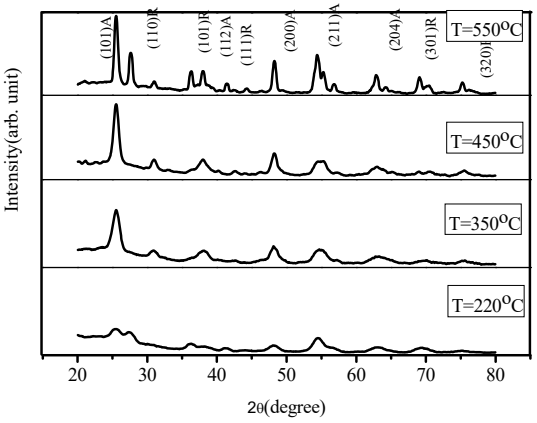

Fig.1a XRD patterns of undoped TiO_2 annealed at different temperatures ranging from 220 to 550°C

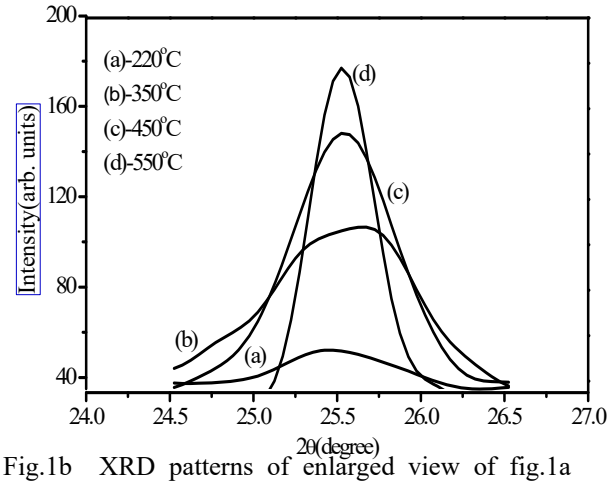

Fig.1b XRD patterns of enlarged view of fig.1a ranging from 24-27 (degree) for undoped TiO_2 annealedat different temperature(220,350,450,550°C).

The XRD patterns of non-aqueous sol-gel synthesized and 220-550°C heat treated samples of 0.0, 0.4, 0.8 and 1at. % Eu^{3+} ion doped and undoped TiO_2 are shown in Fig. 1(a)-(i). The sample exhibits XRD diffraction lines corresponding to the anatase(JCPDS Card No. 86-1157), rutile(JCPDS Card No. 87-0710) and mixed phases of TiO_2(B) (JCPDS Card No. 78-1510).

The as prepared sample is found to be amorphous in nature, which is confirmed by XRD study. When the sample is annealed at 220°C-550°C, crystalline TiO_2 is formed. The XRD pattern vividly shows the tetragonal phase of TiO_2 with lattice parameters a = 3.783Å and c= 9.497 Å with cell volume= 135.91Å (JCPDS Card No. 86-1157). The XRD patterns of the annealed

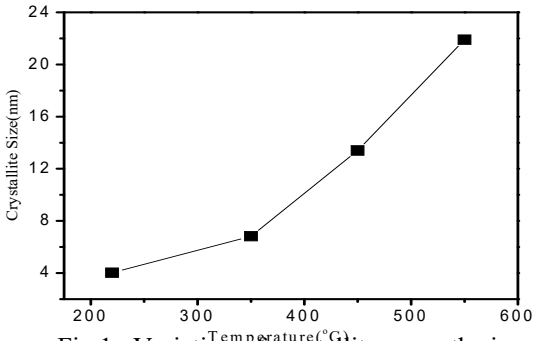

Fig.1c Variation of crystallites growth size of doped TiO_2 at different annealed temperatures.

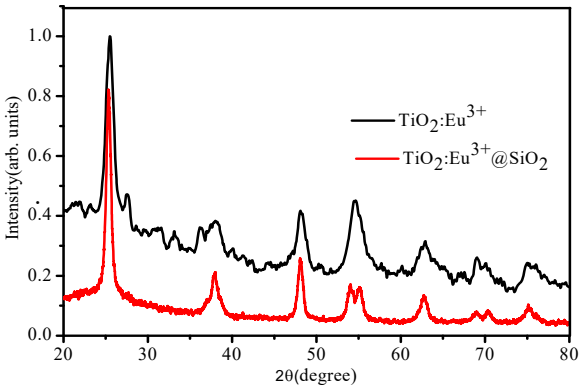

Fig.1d XRD patterns of doped TiO_2:Eu^{3+}(0.4 at. %) and TiO_2:Eu^{3+}@SiO_2(0.4 at. %) nanoparticles.

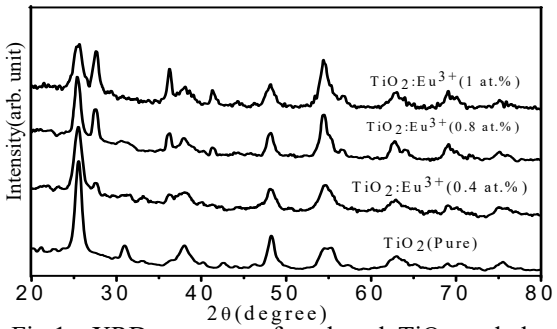

Fig.1e XRD patterns of undoped TiO_2 and doped TiO_2:Eu^{3+}(0.4,0.8 and 1 at. %) nanoparticles.

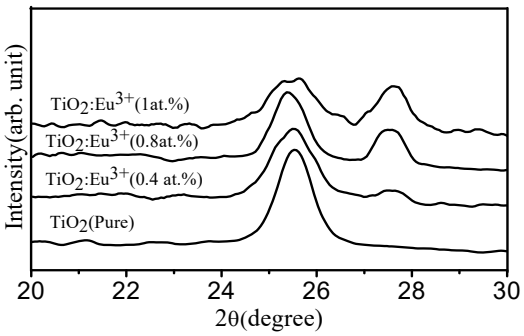

Fig.1f XRD patterns of enlarged view of fig.1e ranging from 24-30 (degree) for undoped TiO_2 and doped TiO_2:Eu^{3+}(0.4,0.8 and 1 at. %).

samples of undoped TiO_2 at different temperatures ranging from 220 to 550°C has been shown in fig. 1(a) with planes of the respective peaks. The graph shows a changing pattern from amorphous to crystalline TiO_2. Fig.1(b) shows XRD patterns of undoped TiO_2 nanoparticles heat treated at different temperature(220, 350, 450, 550°C). Here, the peak intensity of the XRD spectra increases with increase in temperature. It was also found that the width of peaks decreases with the increase of annealed temperatures due to growth of crystals and construction to larger clusters. Variation of crystallites growth of undopedtitania nanoparticles at different annealed temperatures has been shown in fig.1(c). Fig.1d shows the variation of peaks of TiO_2: Eu^{3+} core from TiO_2: Eu^{3+} @SiO_2 core-shell. It has been found that the crystallite size increases with the increase of annealed temperature.

The XRD patterns of 450°C heat treated sample of Eu^{3+} doped in TiO_2 at different concentration 0.4, 0.8 and 1 at.% are shown in fig.1(e). The peaks at 25.5 degree have been chosen and compare at different doping levels (Fig.1f). The peak position increases as the concentration of Eu^{3+} ion doped in TiO_2 increases. New peak appears on the diffractogramas the concentration increases from 0.4 at.% to1 at. % doped Eu^{3+} ion. This is the indication of phase transformation from anatase to rutile. Furthermore the variation of crystallite growth size doped with Eu^{3+} at different concentration on different annealed temperatures has been plotted (fig.1g). We found that the crystallite size decreases as the concentration of doping increases for all temperature ranges. It has also been observed that the crystal size increases as the temperature increases. Debye - Scherer relation (Eqn.2.1) and Williamson-Hall equation (Eqn.2.2) have been used to calculate crystalline size. Table 1 shows the lattice parameters, unit cell volume and crystallite size of nanoparticles using Debye - Scherer relation. Table 2 shows average crystallite size and

strain of the nanoparticle using Williamson-Hall equation.

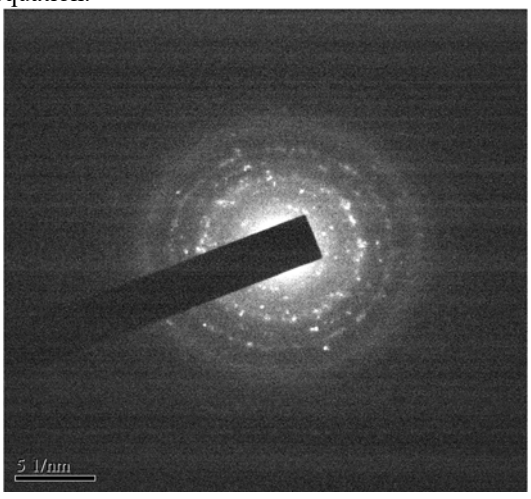

Fig.2a TEM image of TiO_2 annealed at 350°C and its SAED pattern.

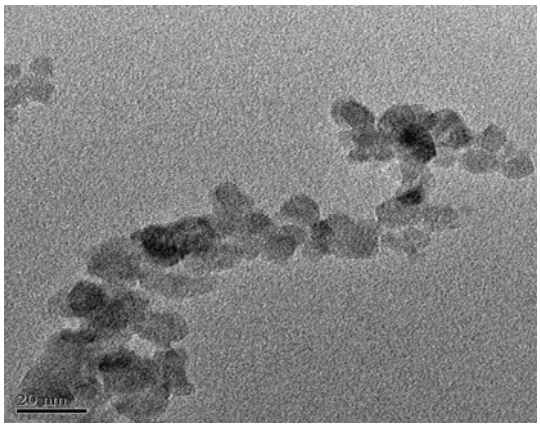

Fig.2bTEM image of TiO_2 annealed at 350°C.

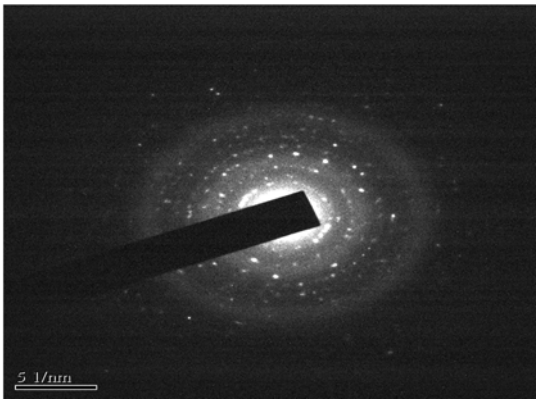

Fig.2cTEM image of TiO_2 annealed at 550°C and its SAED pattern.

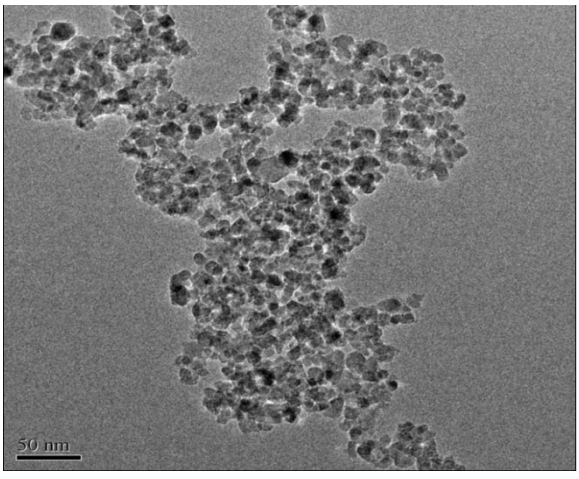

Fig.2dTEM image of TiO_2 annealed at 550°C.

3.1TEM study

Figs. 2(a-d) represent TEM images of TiO_2 nanoparticles after heat treatment at 350°C and 550°C respectively. The particles are found to have spherical shape with size around ~ 11nm at both temperatures as can be seen in the figs 2(b), 2(d). The sizes obtained from TEM are in good agreement with the computed size with the use of Scherrer's relation from XRD data. Fig.2a and fig.2c show the Selected Area Electron Diffraction(SAED) pattern of 350°C and 550°C heated sample of undoped TiO_2. Visible rings in the SAED patterns are assigned to the (101), (004), (200) and (105) planes. The interplanar spacing d_{hkl} calculated from SAED patterns agree well with that of respective crystal planes(JCPDS Card No 86-1157). Figs. 2(e –f) represent TEM size histogram of TiO_2 and annealed at 350°C and 550°C respectively which were found to be 10.9nm and 11.4 nm respectively.

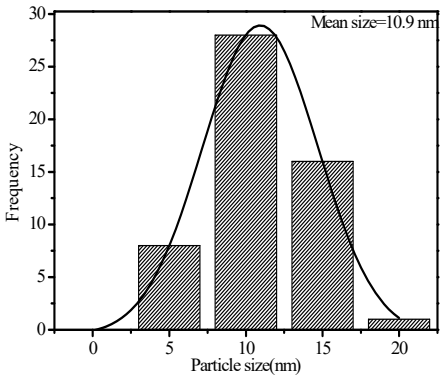

Fig.2e The size distribution histogram of TiO_2 annealed at 350°C.

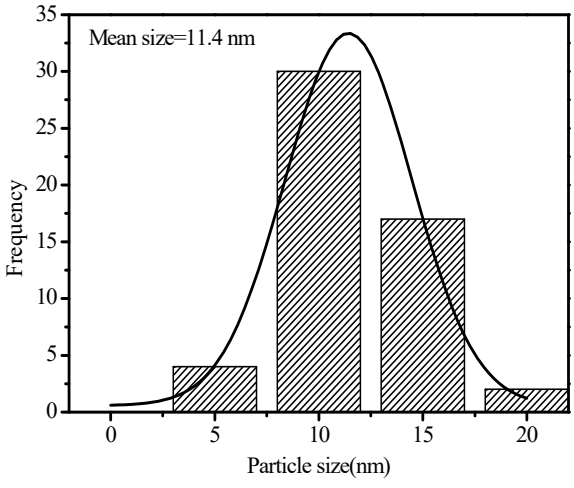

Fig.2f The size distribution histogram of TiO_2 annealed at 550°C

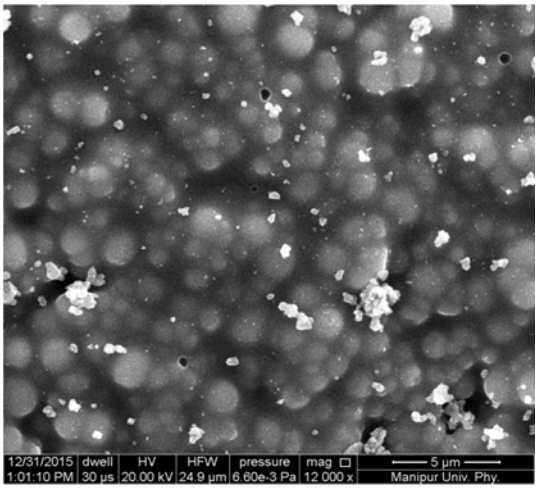

Fig.2g SEM image of TiO_2:Eu^{3+} (0.4 at.%) annealed at 350°C.

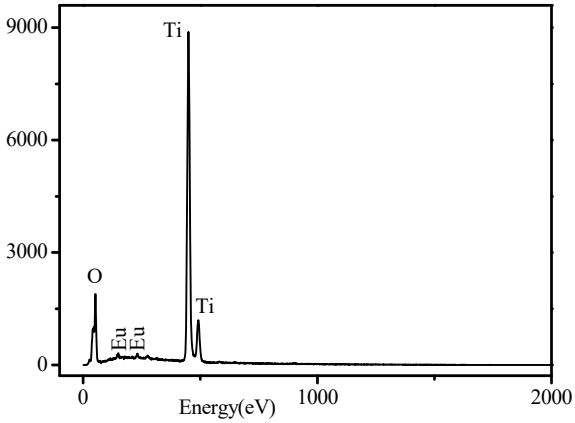

Fig.2h EDX spectra of TiO_2:Eu^{3+} (0.4 at.%) annealed at 350°C.

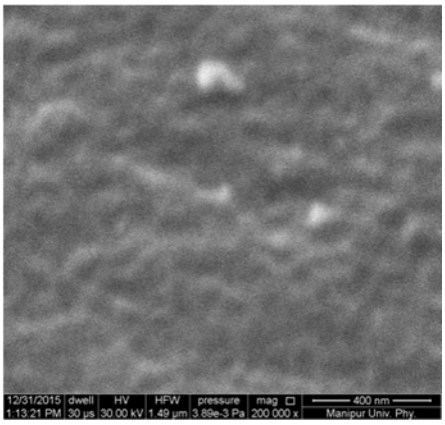

Fig.2iSEM image of TiO_2:Eu^{3+} (0.8 at.%) annealed at 350°C

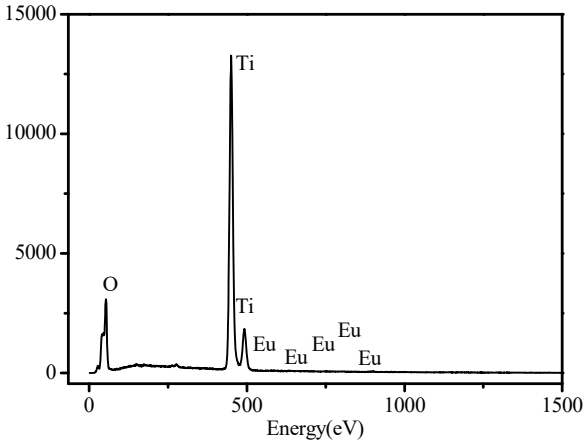

Fig.2jEDX spectra of TiO_2:Eu^{3+} (0.8 at.%) annealed at 350°C.

3.2 SEM and EDX study

The SEM image and EDX[32] of TiO_2: Eu^{3+} (0.4 and 0.8 at.% of Eu^{3+}) at 350°C are shown in fig.2g, fig.2i and fig.2h, fig.2j. The particles are aggregated with small crystals with a broad size distribution upto 4µm and 500 nm respectively. All the SEM images are found to show particles of spherical and even shape. Some spot of impurities are also observed which may be due to the presence of remains of unreacted TIP or may be due to lack of washing. The EDX spectra of Fig.2h and Fig.2j verify the presence of Ti, O and Eu in the prepared sample. The ionic concentrations of titanium and europium of the prepared TiO_2: Eu^{3+} samples are determined using EDX data. The presence of elemental Ti:Eu ratio are observed to be 94.8 and 553.6 respectively for the sample of TiO_2:Eu^{3+}(0.4 and 0.8 at.% of Eu^{3+}). A decrease in the content of titanium and an increase in the relative content of europium are observed with the increasing nominal concentration of the dopant in the samples.

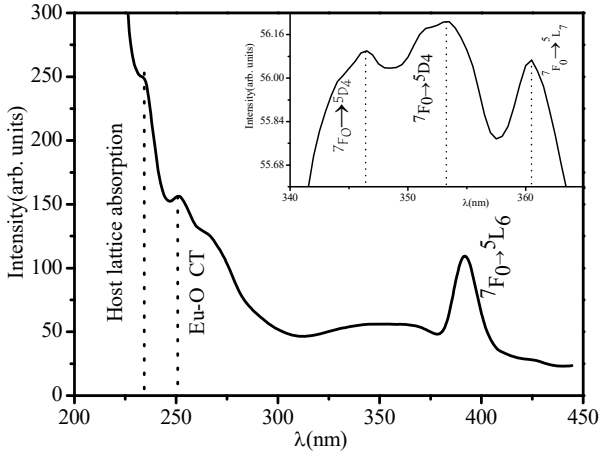

Fig.3a Excitation spectrum of TiO_2 doped with 0.4 at.% of Eu^{3+} ion annealed at 350°C recorded at 532nm emission wavelength and the inset shows the enlarged region around $^7F_0 \rightarrow {}^5L_6$ transition.

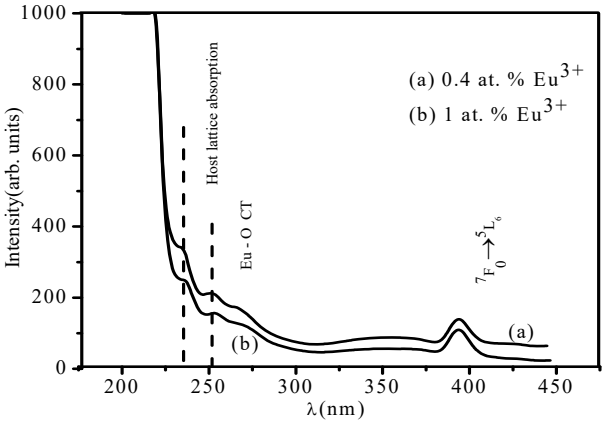

Fig.3bvariation of intensity with the wavelength of Eu^{3+}doped(a-0.4 and b-1 at.%) of titania nanoparticle at 350°C.

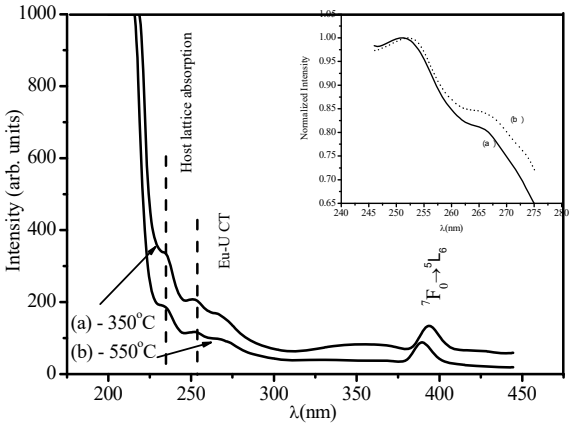

Fig.3cExcitation spectra of TiO_2:Eu^{3+}(0.4 at. %) nanoparticles monitored at 532nm emission wavelength annealing at different temperature. Inset shows the enlarged view of charge transfer region.

Figure 3a is the representative excitation spectrum of TiO_2 doped with 0.4 at.% of Eu^{3+} ion annealed at 350°C recorded at 532nm emission wavelength. The characteristic peaks of the excitation spectrum correspond to the band at 393 nm is attributed to the f-f transitions with the Eu^{3+} $4f^6$ configuration [33]. The low shoulder peak centred at 234nm is attributed to host lattice absorption. The peak bands at 250-251nm correspond to Eu-O charge transfer state (CTS) caused by the electron transferred from the oxygen 2p orbital to the empty 4f orbital of europium, which may be described as ligand-to-Eu^{3+} charge transitions (LMCT)[34,35].The inset is the enlarged region from 340–370 nm of fig.3a encompassing three sets of transition bands assigned to $^7F_0 \rightarrow {}^5D_4$ (346nm), $^7F_0 \rightarrow {}^5D_4$ (352 nm), $^7F_0 \rightarrow {}^5L_7$ (360 nm) respectively. The strongest excitation peak

band at 393nm is due to $^7F_0 \rightarrow {}^5L_6$ transition. This work observed lower value of peak positions as compared to the reported value except band at 393nm [36]. The variation of intensity with the wavelength of Eu^{3+} doped (a-0.4 and b-1 at.%) of titania nanoparticle at 350°C has been shown in fig.3b. The change in excitation intensity and peak position of the photoluminescence were found to observe with the increase of concentration. A slight red shift is found to observe in the charge transfer region at 1 at.%. On the other hand, the PL intensity is very low and does not change significantly at both the concentrations. Fig. 3c shows the change of peak position to longer wavelength (red shift) with the increase of annealing temperature particularly at the $^7F_0 \rightarrow {}^5L_6$ transition whereas host lattice absorption region and charge transfer region are almost in the same state.

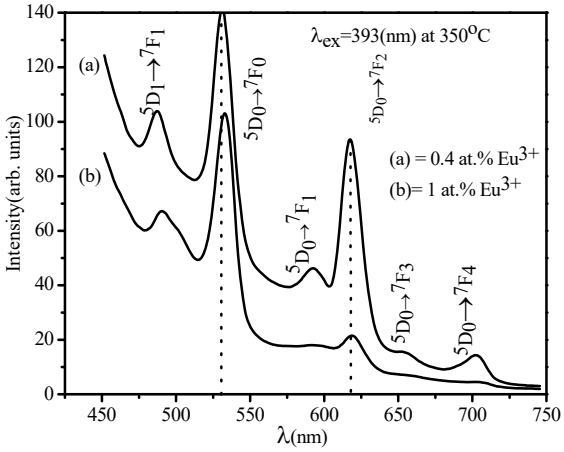

Fig.3dPhotoluminescence emission peaks in the range 486-704nm of TiO_2:Eu^{3+} (0.4 and 1 at.% of Eu^{3+}) nanocrystal monitored at 393nm excitationwavelength annealed at 350°C.

[1]TABLE 1

Sl. No.	Sample	Crystallite Size (nm)	Unit cell parameters		
			a(Å)	c(Å)	Cell volume(Å^3)
1	TiO_2	11.9 ± 0.01	3.783	9.497	135.91
2	TiO_2:Eu^{3+}(0.4%)	7.87 ± 0.01	3.73	9.37	130.36
3	TiO_2:Eu^{3+}(0.8%)	7.52 ± 0.01	3.783	9.51	136.10
4	TiO_2:Eu^{3+}(1.0%)	6.83 ± 0.01	4.594	2.958	162.43

[1] The structure parameters ofTiO_2:Eu^{3+} (0, 0.4, 0.8,1 at. %) annealed at 350°C using Debye - Scherer relation.

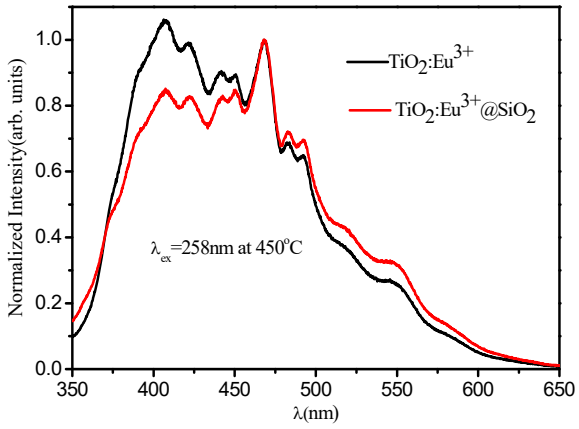

Fig.3ePhotoluminescence emission spectra of TiO_2:Eu^{3+} (0.4 at. % of Eu^{3+}) andTiO_2:Eu^{3+} @SiO_2(0.4 at. % of Eu^{3+}) nanocrystal monitored at 258nmexcitation wavelength annealed at 450°C.

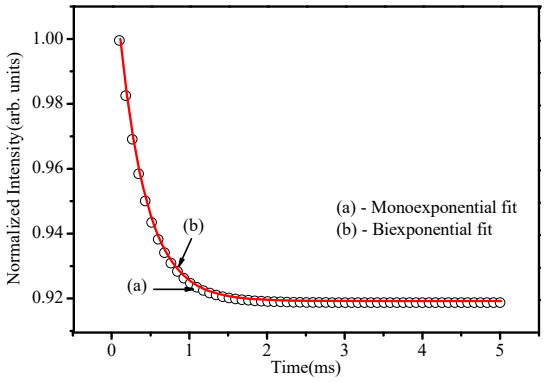

Fig.3g Photoluminescence decay curve for 1at. % Eu^{3+} doped TiO_2 annealed sample at 350°C recorded

at 352nm excited wavelength and at 617nm emission ($^5D_0 \rightarrow {}^7F_2$).

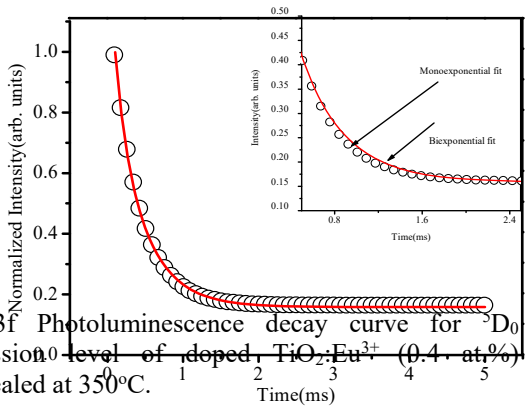

Fig.3f Photoluminescence decay curve for $^5D_0$ emission level of doped TiO_2:Eu^{3+} (0.4 at.%) annealed at 350°C.

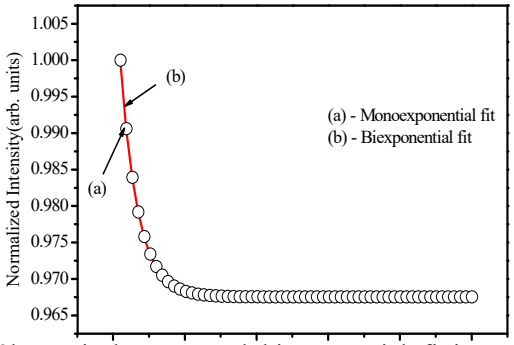

Fig.3h Typical monb and biexponential fitting to decay lifetime spectra of 1 at.% Eu^{3+} doped TiO_2 heat treated at 550°C recorded at 393nm excited wavelength and at 617nm emission ($^5D_0 \rightarrow {}^7F_2$).

TABLE 2

Sl. N0.	Sample	Crystallite Size(d)nm	Strain(η)
1	TiO_2	7	$1.14x10^{-2}$
2	TiO_2:Eu^{3+}(0.4%)	6	$2.23x10^{-2}$
3	TiO_2:Eu^{3+}(0.8%)	4	$2.46x10^{-2}$
4	TiO_2:Eu^{3+}(1.0%)	3	$8.1x10^{-2}$

The structure parameters of TiO_2:Eu^{3+} (0, 0.4, 0.8,1 at. %) annealed at 350°C using Williamson-Hall equation.

TABLE 3

Sl. No.	Sample	350°C Intensity			550°C Intensity		
		$^5D_0 \rightarrow {}^7F_2$(E)	$^5D_0 \rightarrow {}^7F_1$(M)	E/M	$^5D_0 \rightarrow {}^7F_2$(E)	$^5D_0 \rightarrow {}^7F_1$(M)	E/M
1	TiO_2:Eu^{3+}(0.4%)	45.9/591	93/617	0.494	17.8/597.3	21.4/618.8	0.832
2	TiO_2:Eu^{3+}(1.0%)	21.6/594	28.4/617	0.741	5/588	6.4/618.5	0.781

Peak intensities and position of CTS, electric and magnetic dipole transitions of Eu^{3+} in the TiO_2:Eu^{3+} samples. The ratio within the column represents peak intensity and peak position.

3.3 Luminescence study

3.3.1 Excitation study

Figure 3a is the representative excitation spectrum of TiO_2 doped with 0.4 at.% of Eu^{3+} ion annealed at 350°C recorded at 532nm emission wavelength. The characteristic peaks of the excitation spectrum correspond to the band at 234, 250 and 393 nm that are attributed to the f-f transitions with the Eu^{3+} $4f^6$ configuration [33]. The low shoulder peak centred at 234nm attributes host lattice absorption. The peak bands at 250-251nm correspond to Eu-O charge transfer state (CTS) caused by the electron transferred from the oxygen 2P orbital to the empty 4f orbital of europium which may be described as ligand-to-Eu^{3+} charge transitions (LMCT)[34-35].The inset is the enlarged region from 340–370 nm of fig.3a encompassing three sets of transition bands assigned to $^7F_0 \rightarrow {}^5D_4$ (346nm), $^7F_0 \rightarrow {}^5D_4$ (352 nm), $^7F_0 \rightarrow {}^5L_7$ (360 nm) respectively. The strongest excitation peak band at 393nm attributes $^7F_0 \rightarrow {}^5L_6$ transition. This work observed lower value of peak positions as compare to the reported value except band at 393nm [36]. The variation of intensity with the wavelength of Eu^{3+} doped (a-0.4 and b-1 at.%) of titania nanoparticle at 350°C has been shown in

fig.3b. The change in excitation intensity and peak position of the photoluminescence were found to observe with the increase of concentration. A slight red shift is found to observe in the charge transfer region at 1 at.%. On the other hand, the PL intensity is very low and does not change significantly at both the concentrations.

Fig. 3c shows the change of peak position to longer wavelength (red shift) with the increase of annealing temperature particularly at the $^7F_0 \rightarrow ^5L_6$ transition whereas host lattice absorption region and charge transfer region are almost in the same state.

3.3.2 Emission study

Fig. 3d shows the six characteristic PL emission peaks in the range 486-704 nm of TiO_2: Eu^{3+} (0.4 and 1 at.% of Eu^{3+}) nanocrystal monitored at 393nm excitation wavelength annealed at 350ºC. The figure shows strong red emission band at 617 nm attributed to $^5D_0 \rightarrow ^7F_2$ allowed electric dipole transition indicating that the Eu^{3+} ion is located in a noncentrosymmetric position in the matrix and remaining emission peaks are in the visible region [35]. The weak emission peak centred at 592.8 nm assigned to $^5D_0 \rightarrow ^7F_1$ allowed magnetic dipole transition which is insensitive to crystal field environment and other four peaks centred at 486.2, 531, 654.5 and 704 nm assigned to the $^5D_1 \rightarrow ^7F_2$, $^5D_0 \rightarrow ^7F_0$, $^5D_0 \rightarrow ^7F_3$ and $^5D_0 \rightarrow ^7F_4$ transition respectively but $^5D_0 \rightarrow ^7F_4$ transition is very near to the infrared region [35-37]. The electric dipole transition is much stronger than the magnetic dipole transition, suggesting that Eu^{3+} takes a low symmetry site without an inversion centre in the TiO_2 host lattice [38]. The emission peak intensity at 617 nm steeply decreases at 1at.% Eu^{3+}due to concentration quenching effect. This effect comes from cross relaxation among Eu^{3+} ions which increases with decreasing distance between Eu^{3+}- Eu^{3+}[39]. The electric dipole transition depends on environment whereas magnetic dipole transition is independent of environment according to Judd-Ofelt theory [40-41]. The asymmetric ratio of PL (A_{21}) of Eu^{3+} is defined as the ratio of the intensity(I_2) of the electric dipole allowed transition ($^5D_0 \rightarrow ^7F_2$) to the intensity (I_1) of the magnetic allowed dipole transition ($^5D_0 \rightarrow ^7F_1$) [41]. It is very sensitive to the environment around Eu^{3+} ion. Asymmetric ratio A_{21} is found to be 0.494 and 0.832 for 0.4 at. % Eu^{3+} doped TiO_2 sample annealed at 350 and 550ºC respectively. The asymmetric ratio A_{21} of 1 at.% Eu^{3+} doped TiO_2 sample annealed at 350ºC and 550ºC are found to be 0.741 and 0.781 respectively. This increase of asymmetric ratio at different temperatures suggests the dependence of local symmetry of Eu^{3+} [42]. Details are shown in Table 3. Fig. 3e shows the emission spectra of TiO_2: Eu^{3+} core and TiO_2: Eu^{3+}@SiO_2 core-shell. Core- sample and core-shell sample are found to have higher intensity at 406nm and 468nm respectively heat treated at 450ºC. It indicates that during core-shell formation, Eu^{3+} ions available in core diffuse towards the shell so that Eu^{3+} ions are diluted in concentration. From this study we observed, there is no change in peak positions of Eu^{3+} emission with the particle size or heat treatment. From the Commission Internationale de Ìéclairage (CIE) cromacity study, the colour space coordinate of 0.4 at. % Eu^{3+}doped TiO_2 sample annealed at 350ºC monitored at 393 nm excitation wavelength was found to be (0.30, 0.32). For the sample of 1 at.% Eu^{3+}doped TiO_2 treated at the same temperature and excited wavelength,colour coordinate was found to be (0.30, 0.33). From the calculated CIE co-ordinates (x, y), the sample shows emission in the white region of CIE co-ordinate. These samples therefore will be good for the purpose of white light emitting devices.

3.3.3 Lifetime study

Fig. 3(e) illustrates a typical PL decay curve for $^5D_0$ emission level of doped TiO_2 : Eu^{3+} (0.4 at.%) annealed at 350ºC. The luminescence decay is possible to the low concentration lanthanide ion in different matrices as per report [43]. The experimental decay data are fitted both in first order (monoexponential) and second order (biexponential) exponential decay equations [43]:

Monoexponential decay

$$I_t = I_0 \exp(-t/\tau) \qquad (2.7)$$

where I_t is the intensity at time t, I_0 is the intensity at time t=0 and τ is the decay life time.

Biexponential decay

$$I_t = I_1 exp(-t/\tau_1) + I_2 exp(-t/\tau_2) \quad (2.8)$$

where I_1 and I_2 are intensities at different times and τ_1 and τ_2 is their corresponding lifetime. The average lifetime can be determined from the equation [42]

$$\tau_{av} = ((I_1\tau_1^2 + I_2\tau_2^2)/(I_1\tau_1 + I_2\tau_2)) \qquad (2.9)$$

The average value of decay (τ_{av}) is found to be 0.351ms (~351 μs) of 0.4 at.% Eu^{3+} doped TiO_2 sample annealed at 350ºC monitored at 352nm excited wavelength and 617nm emission wavelength, τ_1 and τ_2 are found to be 0.351ms (50% I_t) and 0.351ms (50% I_t) respectively.

A typical graph of intensity as function of time is plotted for 1 at. % Eu^{3+} doped TiO_2 annealed sample at 350ºC recorded at 352nm excited wavelength and at 617 nm emission ($^5D_0 \rightarrow ^7F_2$) shown in fig. 3(f). It is fitted biexponentially and average decay lifetime (τ_{av}) value for this sample is calculated with the use of equation (2.11). Its value is found to be 0.35ms, the same value of τ_1 and τ_2 are found to be 0.35 (50% I_t). The average decay lifetime (τ_{av}) value in the case of monoexponential fitting is also similar to the biexponential fitting. The average value of decay(τ_{av}) is found to be 0.243ms (~243 μs) for biexponential fitting of 1 at.% Eu^{3+} doped TiO_2 sample annealed at 350ºC monitored at 352nm excited wavelength for 617nm emission ($^5D_0 \rightarrow ^7F_2$), τ_1 and τ_2 are found to be 0.243ms (50% I_t) and

0.2431ms (50% I_t) respectively. For TiO_2: Eu^{3+}(1 at. % Eu^{3+}) sample annealed at 550°C excited at 393nm for 617nm emission the average value of decay (τ_{av}) is found to be 0.375ms (~375 μs) for biexponential fitting, τ_1 and τ_2 are found to be 0.407 ms (70% I_t) and 0.129 ms (29% I_t) respectively (Fig.3g). We have observed that the lifetime increase significantly from 243 μs to 375μs, as temperature increases from 350°C to 550°C. This increase in the lifetime is due to decrease in surface defects as the particle size increases with temperature [44-45]. Furthermore, it has been found from figs. (3e-3f) that the lifetime decreases as the concentration of doping level increases, which is of similar pattern with the decrease of luminescence intensity as Eu^{3+} concentration increases.

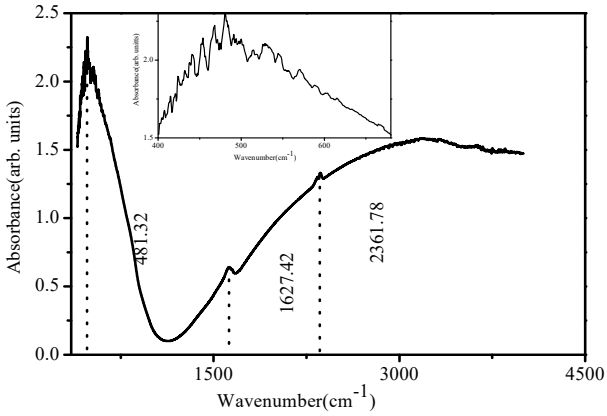

Fig.4aThe FT-IR spectra of undoped TiO_2 annealed at 350°C and inset is the expanded view of lower wavenumber

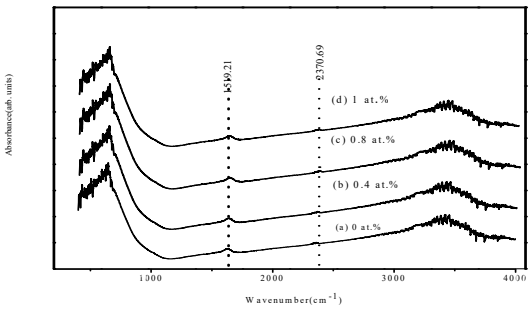

Fig.4bThe FT-IR spectra of undoped and doped TiO_2 :Eu^{3+}annealed at 350°C

3.4 FTIR study

Figs.4(a-b) show the FTIR spectra of undoped TiO_2 annealed at 350°C and the combine spectra of undoped and doped TiO_2: Eu^{3+}annealed at 350°C. In the spectra, the absorption peaks are found at 628.09, 1630.66 and 2365.02 cm^{-1} respectively. Peaks observed at 628.09 cm^{-1} correspond to stretching vibration of Ti-O vibration. Peak observed at 1630.66 cm^{-1} corresponds to C=O vibrations and this is mainly due to the absorption of CO_2 by the gel. Peak observed at 2365.02 cm^{-1} corresponds to C-H stretching vibration. We observed that the peaks shift to higher wavenumber as the concentration of the doping concentration of Eu^{3+} increases. This is an indication of substitutional accommodation of the dopant ion in titania nanoparticles [46].

4.0 Conclusion

Eu^{3+} ion doped and undopedtitania nanocrystals were synthesized by non aqueous sol-gel technique at low temperature and were characterized using (XRD), PL, FTIR and TEM respectively. We could get the crystallite size of the range of 2-9 nm using Williamson-Hall equation, which is consistent with the TEM result. photoluminescence study showed that the lifetime increases significantly as the temperature increases. Furthermore, the lifetime is found to decrease as the concentration of doping level increases. The band gap energy (E_g) of Eu^{3+} doped TiO_2 is found decrease as compared to undoped TiO_2 nanoparticles. The presence of anatase and rutile phases and their transition states from anatase to rutile are also confirmed by FTIR, in addition to XRD data.

Acknowledgements:
The authors are grateful to FIST- DST, Delhi for instrumentation facilities in the Department of Physics, NERIST, Arunachal Pradesh, India.

References:

1. K.Tennakone,G.R.R.A.Kumara,L.R.M.Kottegoda, V.P.S. Perera,et al., J. Photochem. Photobiol.A 117(1998) 137-142.
2. H. Long, A. Chen, G. Yang, Y. Li, et al., Thin Solid Films S17(2009) 5601-5604.
3. Q. Li, S. Mahendra,D.Y.Lyon, et al., Water Res. 42(2008) 4591-4602.
4. D. Deng, G.M.Kim, J.Y.Li, et al.,J.Energy Environ. Sci.m 2(2009) 817-837.
5. G.Wang, H. Wang, Y. Ling, et al., Nano Lett. 11(2011) 3026-3033.
6. X. Chen, L. Liu, P.Y.Yu, et al., Nanocrystals Science, 331(2011) 746-750.
7. Y. Zhang, W.Fu, H. Yang, Q. Qi, et al., Surf. Sci., 254(2008) 5545-5547.
8. M. Zukalova, M. Kalbac, L. Kavan, et al., Chem. Mater. 17(2005) 1248-1255.

9. C.Xu, P.H.Shin, L.Cao, J.Wu, et al., Chem. Mater., 22(2010) 143-148.
10. D.V. Babykin, A.A.Lapkin, P.K.. Plucinski, et al., J. Phys. Chem.B, 109(2005) 19422-19427.
11. GK Das, TT Yang-Tan, J. Phys. Chem.B, 112 (2008) 11211-11217.
12. S. Hongbo, R. Magave, et al., Particle and Fibre Toxicology, 10 (2013) 15-20.
13. K. Liu, X. Lin, J. Zhao, Intl. J. Nanomedicine, 8(2013) 2509-2520.
14. J. Muscat, V. Swamy, N.M.Harrison, Phys. Rev.B, 65(2002) 224112-224115.
15. A. Mills and S. le Hunte, J. Photochemistry and Photobiology A: Chemistry, 108(1997) 1-35.
16. A.J. Kenyon, Prog. Quant. Electron, 26 (2002) 225-284.
17. D. Souz, R.Richrds, Synthesis, Props. And Application of oxide nanoparticles, Whiley,(N.J) Chap.3 2007.
18. S.Buzby, Rs Franklin, S.I. Shah, Synthesis, Props. And Application of oxide nanoparticles, Whiley,(N.J) Chap.4 2007.
19. G.Zeng, Z.J.Ding,Z.M.Zhang, J.Lumin., 118(2006) 301-307.
20. Q.G. Zeng,,Z.J.Ding,Z.M.Zhang, et al., Script. Mater. 57(2007) 897-900.
21. M. Saif, M.S.A Abdel-Mottaleb, Inorg. Chim. Acta. 360(2007) 2863-2874.
22. 22. V. Stengl, S. BakardjievaandN.Murafa, Mater. Chem. Phys., 114(2009)217-226.
23. L.A.Rocha, E.F.Molina,et al., Mater. Chem. Phys., 101(2007)238-241.
24. J.K.Ani, S.Savithri, G.D. Surender,et al., Aerosol and Air Quality Research, 5(2005)1-13.
25. M. Niederberger, Acc. Chem. Res. 40(2007) 793-800.
26. L.Chen,K.Chen,S.Hu,R.Liu, J.Mater.Chem., 21(2011) 3677-3685.
27. G.K.Williamson, W.Hall, ActaMetallurgica, 1(1953) 22-31.
28. R.A.Spurr, H.Mayers, Analytical Chemistry, 29(1957) 760-762.
29. S. Gao, L. Pang, H. Che and X. Zhou, China Particuology, 2(2004) 177-181.
30. X. Zhong, B. Yang, X. Zhang , J. Jia and G. Yi, Particuology, 10(2012) 365-370.
31. A. Gaber, M. A. Abdel-Rahim, A. Y. Abdel-Latief and M. N. Abdel-Salam, Int. J. Electrochem. Sci., 9(2014)81-95.
32. M. Pal, U. Pal, J.M Gracia, Y. Jimenez and F. Pérez- Rodriguez, Nano Reseach Letters,7(2012) 1
33. Baoshun Liu, Liping Wen, Xiujian Zhao, Materials Chemistry and Physics, 106(2007)350-353.
34. M.Yun, W. Zhang, S. Xia, J.C. Krupa, J.Lum., 68(1996)335-339.
35. K. Riwotzki, M. Haase, J.Phys. Chem. D,102(1998)10129-10135.
36. A. Podhorodecki, G .Zatryb, P. Sitarek, et al., Thin Solid Films, 517(2009)6331-6333.
37. A. Conde-Gallardo, M. Garcia-Rocha,I. Hamandez-Calderon, et al., Appl. Phys. Lett., 78(2001)3436-3438.
38. M. Borlaf, M. T. Colomer, R. Moreno, and A.de Andres, J. Am. Ceram. Soc., 98(2015)338-345.
39. R Schmechel, M Kenndy, H V Seggern, et al.,J. Appl. Phys.89 (2001)1679-1686.
40. B.R. Judd, Physical Review, 127(1962)750-761.
41. G.S.Ofelt, Journal of Chemistry and Physics 37(1962) 511-520.
42. B.K.Moon, I.M.Kwon, J.H.Jeong, et al., J.Lumin., 122/123(2007)855-857.
43. M. Yu, J. Lin and J. Fang, Chem. Mater., 17(2005)1783-1791.
44. D.H.Kim, S.H.Kim, K.Lavery, T.P. Russel, Nano. Lett., 4 (2004)1841-1844.
45. N.S.Singh,R.S.Ningthoujam,M. N.Luwang, S. D. Singh, R.K. Vatsa, Chem. Phys. Lett., 480(2009)237–242.
46. M.A. Hamza, F.N. Saiof, A.S. Al-ithawi, et al,Advances in Materials Physics and Chemistry, 3(2013) 174-177.